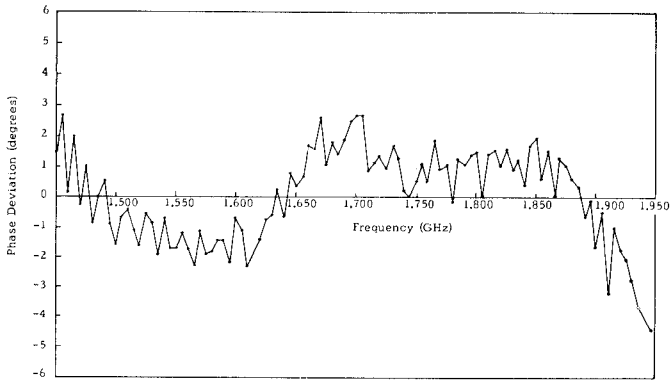

Fig. 5. Phase deviation from linear for the 4-μs L-band delay line.

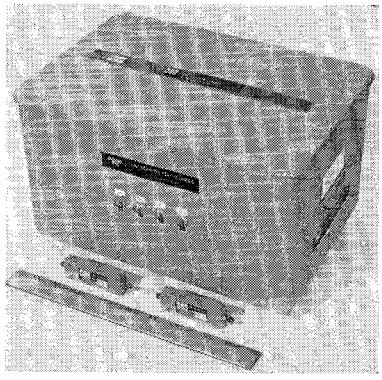

Fig. 6. Photograph showing the identical 4-μs L-band delay lines and temperature stabilizing oven.

the input transducer aperture, at the position of the output transducer aperture. The null location is frequency dependent; thus the angle is determined at the center operating frequency. Theory for propagation along the C axis of sapphire (including the anisotropy) predicts that 33-dB TTS can be achieved over a 33.2-percent bandwidth using this geometrical loss technique. For the 4-μs delay line, with a bevel angle of 43.2 min, TTS in excess of 46 dB is achieved over the 500 MHz centered at 1.7 GHz, as shown in Fig. 4.

The beveled end face, however, increases the loss of the desired delay signal and causes a loss slope with frequency. For the 4-μs delay line with a 43.2-min angle the additional loss incurred due to the angle is 6 dB at 1.45 GHz and 13 dB at 1.95 GHz. This loss slope plus the slight increase in slope due to the propagation loss dependence on frequency is compensated by the diffraction loss due to the input transducer aperture plus tuning to give the flat insertion loss response shown in Fig. 4. The insertion loss of this unit, which averages 30 dB, is flat within 0.5 dB over the 500-MHz bandwidth centered at 1.7 GHz.

Since the delay medium is nondispersive, the phase characteristic of a microwave acoustic delay line would be linear except for phase ripple caused by the acoustoelectric transducers and associated coupling networks, or, in CW operation, by the presence of a triple-transit signal. The phase ripple of a passive network is low if the insertion loss is close to a maximally flat response [9]. For TTS greater than 45 dB, the phase ripple in CW operation due to the triple-transit signal is less than 0.5°. Tuning the matching network for maximally flat response yielded a phase ripple, for the 4-μs delay line, of less than $\pm 2.5°$ from linearity as shown by the data of Fig. 5.

If it is to be useful in microwave systems, a delay line must be packaged with a suitably stable mechanical and thermal environment. The package must also provide shielding to suppress unwanted electromagnetic feedthrough. To determine the necessary thermal environment, CW phase measurements were made on the 4-μs delay line when enclosed in an oven with temperature stability of 0.01°C. The test frequency was stabilized to one part in 10^9 and measured to better than one part in 10^7. Phase was measured with a network analyzer to $\pm 0.6°$. For the 4-μs delay line, which has a path length of approximately 2.4×10^6 degrees, it was found that an oven stability within 0.01°C was necessary to limit the insertion phase drift to $\pm 1°$. Fig. 6 is a photograph of two identical 4-μs delay lines with the characteristics described here, plus a constant temperature oven used to mount the delay lines to limit the phase drift to less than $\pm 5°$ with ambient temperature changes of ± 5°C.

Thus wide-band microwave acoustic delay lines with exceptionally smooth phase and loss responses can be achieved by careful attention to the design techniques described here. These techniques were utilized in achieving 4-μs delay lines with insertion loss of 30 ± 0.5 dB over the 500-MHz band centered at 1.7 GHz, with TTS greater than 45 dB, and with phase deviation from linearity of less than $\pm 2.5°$.

References

[1] F. A. Olson, "Today's microwave acoustic (bulk wave) delay lines," *Microwave J.*, vol. 13, Mar. 1970, pp. 67–76.
[2] N. F. Foster, G. A. Coquin, G. A. Rozgonyi, and F. A. Vannatta, "Cadmium sulphide and zinc oxide thin-film transducers," *IEEE Trans. Sonics Ultrason.*, vol. SU-15, Jan. 1968, pp. 28–41.
[3] T. M. Reeder and D. K. Winslow, "Characteristics of microwave acoustic transducers for volume wave excitation," *IEEE Trans. Microwave Theory Tech.*, vol. MTT-17, Nov. 1969, pp. 927–941.
[4] E. K. Kirchner and R. A. Wilson, "Manufacturing technology for superior microwave acoustic transducers," A.F. Materials Lab., A.F. Syst. Command, Wright-Patterson AFB, Ohio, Tech. Rep. AFML-TR-70-99, June 1970.
[5] H. W. Bode, *Network Analysis and Feedback Amplifier Design*. New York: Van Nostrand, 1945, pp. 360–70.
[6] R. M. Fano, "Theoretical limitations on the broadband matching of arbitrary impedances," *J. Franklin Inst.*, vol. 249, Jan.–Feb. 1950, pp. 57–84 and 139–154.
[7] G. L. Matthaei *et al.*, *Microwave Filters, Impedance Matching Networks, and Coupling Structures*. New York: McGraw-Hill, 1964, ch. 11.
[8] T. M. Reeder and F. A. Olson, "Wideband impedance matching of microwave transducers," presented at 1968 IEEE Ultrasonics Symp., New York, Sept. 1968, Paper L-8.
[9] F. E. Terman, *Radio Engineering*. New York: McGraw Hill, 1947, ch. 6.

The Ring-Loaded Corrugated Waveguide

YOSHIHIRO TAKEICHI, TSUTOMU HASHIMOTO, AND FUMIO TAKEDA

***Abstract*—The ring-loaded corrugated waveguide is shown to be very effective for frequency broadbanding of the waveguide and improvement of the transformer between the corrugated and uncorrugated waveguides.**

I. Introduction

The ring-loaded corrugated waveguide is one devised for the improvement of characteristics of the conventional corrugated waveguide. The corrugated waveguide is applied to the primary horn of a reflector antenna for satellite-communication earth stations to achieve higher efficiency and lower noise temperature [1], [2], but the useful frequency bandwidth of the conventional corrugated waveguide, in which it is effective for the improvement of antenna property, is restricted to about one octave. Besides this, useful frequency bandwidth becomes narrower if good matching is required between the corrugated and uncorrugated waveguides. In the ring-loaded corrugated waveguide, the useful frequency bandwidth is about 1.8

Manuscript received May 3, 1971; revised July 19, 1971.
The authors are with the Mitsubishi Electric Corporation, Kamakura City, Japan.

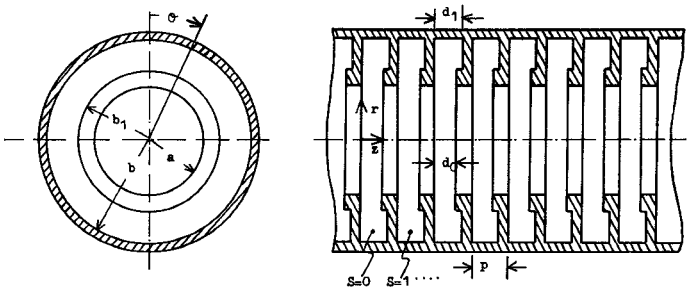

Fig. 1. Ring-loaded corrugated waveguide.

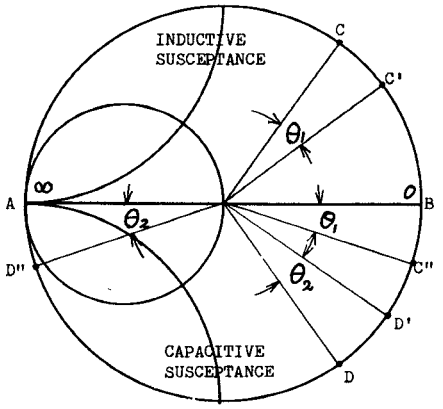

Fig. 2. Admittance chart.

times broader than that in the conventional corrugated waveguide. Moreover, a very broad-band transformer is obtained by applying the ring-loaded corrugated waveguide to the matching section.

II. Theory of the Ring-Loaded Corrugated Waveguide

The structure of the ring-loaded corrugated waveguide is shown in Fig. 1, where a is the inner radius of the fins, b is the radius to the bottom of slots, b_1 is the outer radius of the rings, p is the slot pitch, d_1 is the width of slots, and (d_1-d_0) is the thickness of rings. Rings are added to the fins of the conventional corrugated waveguide. For EH_{11} wave propagating in the corrugated waveguide, which is useful for the improvement of antenna property, the useful frequency bandwidth is restricted to the frequency range in which the slot admittance $\overleftarrow{Y}_{S2}$ at $r=a$ is capacitive [3]. Therefore, the frequency broadbanding of the corrugated waveguide is achieved by expanding the frequency range in which $\overleftarrow{Y}_{S2}$ is capacitive.

In the conventional corrugated waveguide, if the lower edge frequency and the upper edge frequency of the useful frequency bandwidth are designated f_L and f_H, respectively, then the slot admittance $\overleftarrow{Y}_{S2}$ is located at point B at f_L and at point A at f_H on the admittance chart shown in Fig. 2, and $\overleftarrow{Y}_{S2}$ at frequency $f_1(f_L<f_1<f_H)$ is located at a point on the arc $\widehat{ADB}$. In the ring-loaded corrugated waveguide, let Y_{10} and Y_{20} be the characteristic admittances of the ring-unloaded region and the ring-loaded region of a slot, respectively, then $Y_{10}<Y_{20}$. $(b-b_1)$ is chosen so that the slot admittance, as seen at $r=b_1+0$ towards the bottom of the slot, is inductive at frequency f_L and capacitive at frequency f_H, respectively, and it is located at point C at f_L and D at f_H in Fig. 2. Then, according to the relation $Y_{10}<Y_{20}$, the slot admittance, as seen at $r=b_1-0$ towards the bottom of the slot, rotates clockwise at frequency f_L and anticlockwise at frequency f_H on the admittance chart and is located at point C' at f_L and D' at f_H. Therefore, the slot admittance $\overleftarrow{Y}_{S2}$ at $r=a$ is located at point C'' at f_L and D'' at f_H.

By loading fins of the conventional corrugated waveguide with rings to satisfy the preceding condition, the frequency range in which the slot admittance $\overleftarrow{Y}_{S2}$ is capacitive becomes broader than that in the conventional corrugated waveguide.

To make the above concept more clear, the field analysis was performed. In the analysis, the slot pitch p is assumed to be sufficiently small compared to the wavelength, so that the higher order evanescent waves in the slots may be neglected [1], [4].

Now the frequency range of $k>\beta_0$ is considered, $k=2\pi/\lambda$, $\beta_0=2\pi/\lambda_g$, λ and λ_g are wavelengths in free space and the ring-loaded corrugated waveguide, respectively. Then space harmonics may be neglected. The field components in the ring-loaded corrugated waveguide shown in Fig. 1 are expressed as follows, where discontinuity capacitance at $r=b_1$ is neglected.

Region 1, $b_1\leq r\leq b$,

$$
\begin{aligned}
{}_1E_r &= {}_1E_\theta = 0\\
{}_1E_Z &= A_0 V_{m0}(kr)\cos(m\theta)e^{-j\beta_0 sp}\\
{}_1H_r &= A_0\frac{m}{jkr}\sqrt{\frac{\epsilon_0}{\mu_0}}V_{m0}(kr)\sin(m\theta)e^{-j\beta_0 sp}\\
{}_1H_\theta &= -A_0 j\sqrt{\frac{\epsilon_0}{\mu_0}}V_{m0}'(kr)\cos(m\theta)e^{-j\beta_0 sp}\\
{}_1H_Z &= 0.
\end{aligned}
\tag{1}
$$

Region 2, $a\leq r\leq b_1$,

$$
\begin{aligned}
{}_2E_r &= {}_2E_\theta = 0\\
{}_2E_Z &= B_0 U_{m0}(kr)\cos(m\theta)e^{-j\beta_0 sp}\\
{}_2H_r &= B_0\frac{m}{jkr}\sqrt{\frac{\epsilon_0}{\mu_0}}U_{m0}(kr)\sin(m\theta)e^{-j\beta_0 sp}\\
{}_2H_\theta &= -B_0 j\sqrt{\frac{\epsilon_0}{\mu_0}}U_{m0}'(kr)\cos(m\theta)e^{-j\beta_0 sp}\\
{}_2H_Z &= 0.
\end{aligned}
\tag{2}
$$

Region 3, $0\leq r\leq a$,

$$
\begin{aligned}
{}_3E_r &= -\left[C_0\frac{j\beta_0}{k_0}Z_{m0}'(k_0r)+D_0\frac{jkm}{k_0^2r}\sqrt{\frac{\mu_0}{\epsilon_0}}Z_{m0}(k_0r)\right]\cos(m\theta)e^{-j\beta_0 Z}\\
{}_3E_\theta &= \left[C_0\frac{j\beta_0 m}{k_0^2r}Z_{m0}(k_0r)+D_0\frac{jk}{k_0}\sqrt{\frac{\mu_0}{\epsilon_0}}Z_{m0}'(k_0r)\right]\sin(m\theta)e^{-j\beta_0 Z}\\
{}_3E_Z &= C_0 Z_{m0}(k_0r)\cos(m\theta)e^{-j\beta_0 Z}\\
{}_3H_r &= -\left[D_0\frac{j\beta_0}{k_0}Z_{m0}'(k_0r)+C_0\frac{jkm}{k_0^2r}\sqrt{\frac{\epsilon_0}{\mu_0}}Z_{m0}(k_0r)\right]\sin(m\theta)e^{-j\beta_0 Z}\\
{}_3H_\theta &= -\left[D_0\frac{j\beta_0 m}{k_0^2r}Z_{m0}(k_0r)+C_0\frac{jk}{k_0}\sqrt{\frac{\epsilon_0}{\mu_0}}Z_{m0}'(k_0r)\right]\cos(m\theta)e^{-j\beta_0 Z}\\
{}_3H_Z &= D_0 Z_{m0}(k_0r)\sin(m\theta)e^{-j\beta_0 Z}
\end{aligned}
\tag{3}
$$

where

$$
\begin{aligned}
k_0 &= \sqrt{k^2-\beta_0^2}\\
V_{m0}(kr) &= \frac{J_m(kr)Y_m(kb)-J_m(kb)Y_m(kr)}{J_m(kb_1)Y_m(kb)-J_m(kb)Y_m(kb_1)}\\
V_{m0}'(kr) &= \frac{J_m'(kr)Y_m(kb)-J_m(kb)Y_m'(kr)}{J_m(kb_1)Y_m(kb)-J_m(kb)Y_m(kb_1)}\\
m &= 0,\ \pm1,\ \pm2,\ \cdots\\
S &= 0,\ \pm1,\ \pm2,\ \cdots\\
U_{m0}(kr) &= \frac{J_m(kr)+F_0Y_m(kr)}{J_m(kb_1)+F_0Y_m(kb_1)}\\
U_{m0}'(kr) &= \frac{J_m'(kr)+F_0Y_m'(kr)}{J_m(kb_1)+F_0Y_m(kb_1)}\\
Z_{m0}(k_0r) &= J_m(k_0r)/J_m(k_0a)\\
Z_{m0}'(k_0r) &= J_m'(k_0r)/J_m(k_0a)\\
D_0 &= -\frac{\beta_0 a}{ka}\cdot\frac{m}{k_0a}\cdot\sqrt{\frac{\epsilon_0}{\mu_0}}\cdot\frac{1}{Z_{m0}'(k_0a)}C_0
\end{aligned}
$$

A_0, B_0, C_0, D_0, F_0 field amplitude coefficients;
$J_m(x)$ Bessel function of first kind and order m;
$Y_m(x)$ Bessel function of second kind and order m,
$J_m'(x)$, $Y_m'(x)$ first differentials of $J_m(x)$ and $Y_m(x)$ with respect to x;
μ_0 permeability of free space;
ϵ_0 permittivity of free space.

The boundary conditions are given as follows:

$$\overleftarrow{Y_{S2}} = \overrightarrow{Y_{S3}}, \qquad \text{at } r = a$$

$$\overleftarrow{Y_{S1}} = \overrightarrow{Y_{S2}}, \qquad \text{at } r = b_1 \tag{4}$$

where

$$\overleftarrow{Y_{S1}} = \frac{-b_1 \int_0^{d_1}\int_0^{2\pi} [{}_1E_Z \cdot {}_1H_\theta]_{r=b_1} d\theta dZ}{\left[\int_0^{d_1} {}_1E_Z dZ\right]^2_{r=b_1,\theta=0}} \tag{5}$$

$$\overrightarrow{Y_{S2}} = \frac{b_1 \int_0^{d_0}\int_0^{2\pi} [{}_2E_Z \cdot {}_2H_\theta]_{r=b_1} d\theta dZ}{\left[\int_0^{d_0} {}_2E_Z dZ\right]^2_{r=b_1,\theta=0}} \tag{6}$$

$$\overleftarrow{Y_{S2}} = \frac{-a \int_0^{d_0}\int_0^{2\pi} [{}_2E_Z \cdot {}_2H_\theta]_{r=a} d\theta dZ}{\left[\int_0^{d_0} {}_2E_Z dZ\right]^2_{r=a,\theta=0}} \tag{7}$$

$$\overrightarrow{Y_{S3}} = \frac{a \int_0^{p}\int_0^{2\pi} [{}_3E_Z \cdot {}_3H_\theta]_{r=a} d\theta dZ}{\left[\int_0^{p} {}_3E_Z dZ\right]^2_{r=a,\theta=0}}. \tag{8}$$

From (1), (2), (3), and (4), characteristic equation is obtained as follows:

$$j\frac{ka\pi}{p}\sqrt{\frac{\epsilon_0}{\mu_0}}\left[\frac{1}{k_0} Z_{m0}'(k_0 a) - \frac{m^2}{k_0}\left(\frac{\beta_0 a}{k_0 aka}\right)^2 \frac{1}{Z_{m0}'(k_0 a)}\right]$$

$$= j\frac{ka\pi}{d_0}\sqrt{\frac{\epsilon_0}{\mu_0}}\left[\frac{\frac{d_0}{d_1}\frac{\delta_m(ka, kb_1)}{\delta_m(kb_1, ka)}\frac{V_{m0}'(kb_1)}{k} - \frac{\delta_m'(kb_1, ka)}{k\cdot\delta_m(kb_1, ka)}}{1 + \frac{d_0}{d_1}\frac{\xi_m(ka, kb_1)}{\delta_m(kb_1, ka)}}\right] \tag{9}$$

where

$$\xi_m(x, y) = J_m(x)Y_m(y) - J_m(y)Y_m(x)$$
$$\delta_m(x, y) = J_m'(x)Y_m(y) - J_m(y)Y_m'(x)$$
$$\delta_m'(x, y) = J_m'(x)Y_m'(y) - J_m'(y)Y_m'(x).$$

From the above equations, the right-hand side of (9) is easily found to be identical to $\overleftarrow{Y_{S2}}$, the slot admittance as seen at $r=a$ towards the sth slot.

In Fig. 3 the variation of the useful frequency bandwidth is shown for variation of (b_1-a) as an example of the numerical results. The solid curves and dashed curves show the variations of the useful frequency bandwidths in the ring-loaded corrugated waveguide and the conventional corrugated waveguide, respectively. It is seen from this figure that the useful frequency bandwidth of the ring-loaded corrugated waveguide becomes maximum at $(b_1-a)/(b-a)$ of about 0.25 and 1.8 times broader than that of the conventional one.

III. Application to the Matching Section

In order to obtain good property in the matching section between the corrugated and uncorrugated waveguides, it is necessary that the slot admittance $\overleftarrow{Y_{S2}}$ of the corrugated waveguide is near to the wall admittance of the uncorrugated waveguide. Therefore, good matching is obtained by making the slotwidth of the corrugated waveguide progressively narrow towards the uncorrugated waveguide, but in this case the frequency f_L at which the slot admittance $\overleftarrow{Y_{S2}}=0$ remains constant, so the matching is difficult at and near frequency f_L.

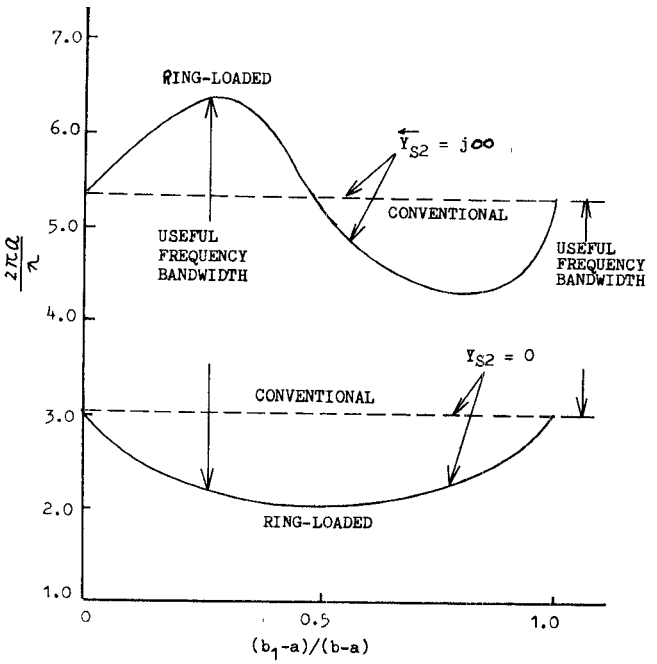

Fig. 3. Useful frequency bandwidth for $(b_1-a)/(b-a)$. $b/a=1.583$, $p/a=0.36$, $d_0/a=0.0257$, $d_1/a=0.103$.

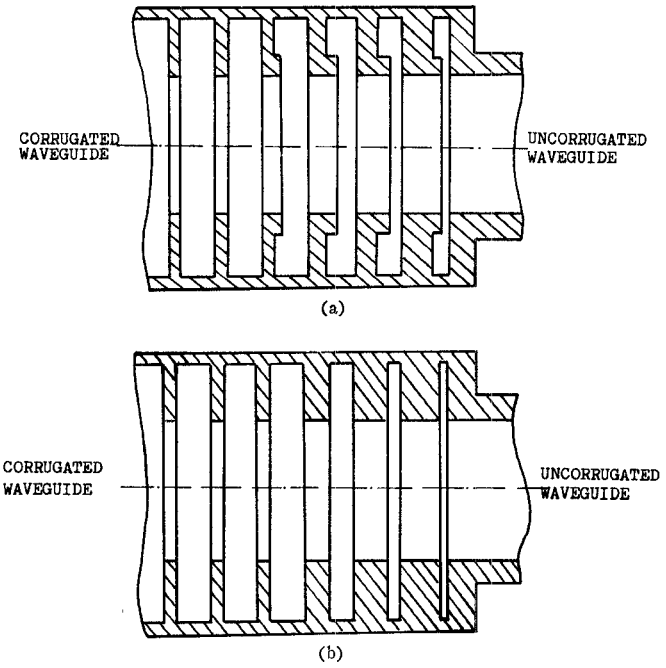

Fig. 4. Transformers between the corrugated waveguide and uncorrugated waveguide.

In the ring-loaded corrugated waveguide, frequency f_L' at which $\overleftarrow{Y_{S2}}=0$ is lower than f_L, as shown in Fig. 3, and the slot admittance $\overleftarrow{Y_{S2}}$ at f_L is larger than that in the conventional corrugated waveguide. Thus good matching is obtained even at the frequency f_L.

In Fig. 4 two types of transformers between the corrugated and uncorrugated waveguides are shown. The transformer in Fig. 4(a) contains the ring-loaded corrugated waveguide and the transformer in Fig. 4(b) contains the conventional corrugated waveguide with the narrow slotwidth. In Fig. 5 the experimental results are shown for these transformers. It is seen from this figure that the useful fre-

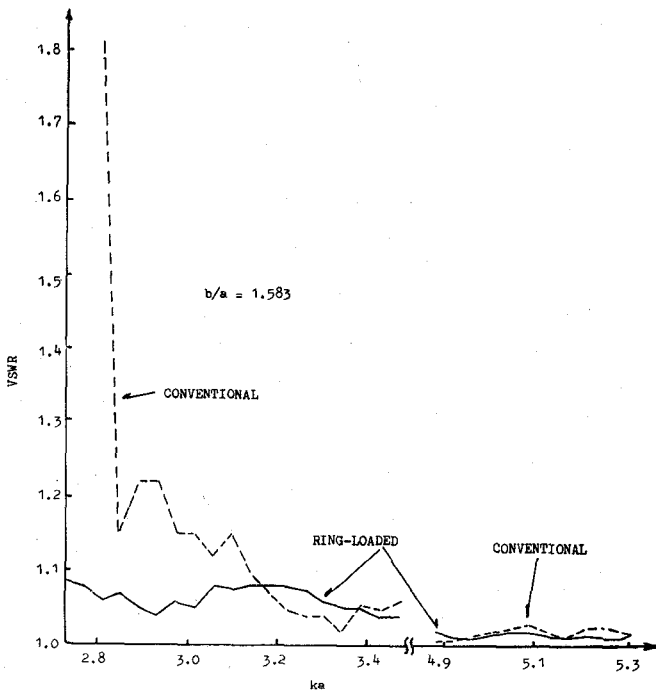

Fig. 5. VSWR for the transformers shown in Fig. 4(a) and (b).

quency bandwidth of the transformer made of ring-loaded corrugated waveguide section is remarkably broader than that of the conventional transformer.

IV. Conclusion

The ring-loaded corrugated waveguide is shown to be very effective for frequency broadbanding of the corrugated waveguide and improvement of the transformer between the corrugated and uncorrugated waveguides.

References

[1] G. H. Bryant, "Propagation in corrugated waveguide," *Proc. Inst. Elec. Eng.*, vol. 116, Feb. 1969, p. 203.
[2] P. J. B. Clarricoats, "Theoretical analysis of cylindrical hybrid modes in a corrugated horn," *Electron. Lett.*, vol. 5, May 1969, p. 187.
[3] A. F. Kay, "The scalar feed," TRG Sci. Rep. 5, 1964, Appendix A1, prepared for Air Force Cambridge Research Laboratories, Office of Aerospace Research, Bedford, Mass., under Contract AF 19(604)-8057.
[4] G. Saxon, T. R. Jarvis, and I. White, "Angular-dependent modes in circular corrugated waveguide," *Proc. Inst. Elec. Eng.*, vol. 110, Aug. 1963, p. 1365.

Controllable Liquid Artificial Dielectrics

H. T. BUSCHER, R. M. McINTYRE, AND S. MIKUTEIT

***Abstract*—A novel approach to microwave phase control, utilizing liquid artificial dielectrics, is described. These media have been fabricated with permittivities which vary in magnitude and anistropy according to the strength of an applied electric control field. Continuously controlled permittivity increases of at least 20 percent in the electric field direction are realizable in liquid suspensions having low loss and very high dielectric strength. A simple waveguide liquid dielectric phase shifter has been built at *Ku* band and its operating characteristics measured. This approach can be applied to the design of electrically variable microwave lenses, power dividers, and resonant cavities as well as phase shifters.**

Manuscript received May 7, 1971; revised July 16, 1971.
The authors are with General Dynamics' Electro Dynamic Division, San Diego, Calif.

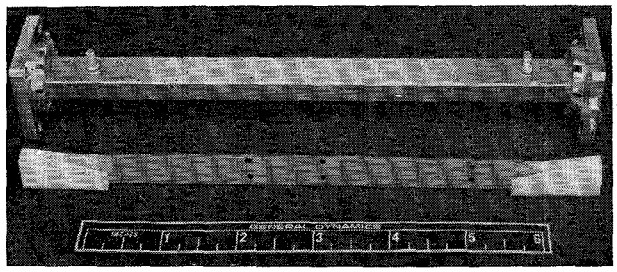

Fig. 1. Phase shifter, showing main control electrode and impedance matching wedges.

Introduction

In connection with phased array research, there has been considerable interest in developing low-cost electronically controlled microwave phase shifters. An economical way to accomplish this is to find a good dielectric with electrically controllable permittivity that can be inserted in the signal path and biased to cause the desired phase delays. This correspondence describes work with suspensions of metallic particles in high dielectric strength liquids. Such suspensions were found to constitute a class of dielectrics with sufficiently large microwave Kerr effect to be useful in practical devices. The physical mechanism of the dielectric's operation is outlined and performance data are presented for a 360° *Ku*-band waveguide phase shifter utilizing the Kerr effect in a liquid suspension [1].

Discussion

The permittivities of the media investigated could be changed by applying a low-frequency electric biasing field. The physical interaction responsible was similar to the one that occurs between light and pure liquids in the optical Kerr effect. In essence, suspensions were constructed as models of Kerr liquids scaled to the microwave region. While the controllable birefringence of a pure Kerr liquid is due to polarization and ordering of its molecules by an applied electric field, the artificial dielectrics used for this study achieved variable microwave birefringence as a result of induced polarization and alignment of their relatively larger solid components. Thus the asymmetric micron-size suspended solids corresponded to individual molecules of a pure Kerr liquid.

Early in this work, a brief search was made for simple liquids composed of large molecules which could show a directly useful Kerr effect at microwave frequencies. Such liquids may exist, but the suspension modeling approach quickly uncovered enough new ground to fully occupy available research personnel.

In order to simultaneously optimize suspension stability and response time, the addition of surfactants was found to be required. Some of these surface-active chemicals, however, tended to increase losses. Searching for components that minimized the cost of this sort of tradeoff produced two practical artificial dielectrics. Both were electrically similar, but one used fluorocarbon and the other hydrocarbon components. The data presented here are based on the more easily reproducible hydrocarbon system, made of benzene loaded with 8 mg/cm³ of 1-μ diameter aluminum platelets and 16 mg/cm³ of alkyl polyoxyethylene-amine.

All measurements were made using the cell shown in Fig. 1, which was designed as a *Ku*-band phase shifter. The electrode shown in front of the cell was normally supported in the *H* plane in the center of the guide, with a fine wire connecting it to an external feedthrough. When voltage was applied to the lead an electric field was impressed on the artificial dielectric in the microwave *E* plane. This caused an increase in permittivity for the TE_{10} mode, so propagation time for that mode increased with applied voltage. Liquid was retained in the guide by thin Mylar end windows. The Teflon wedges shown tapered the liquid column and thereby afforded a smooth impedance transition to the rest of the circuit.

The developmental artificial dielectrics described here underwent gradual settling if left at rest. To avoid this, they were cir-